Journal of Alloys and Compounds 509 (2011) 94–98

Contents lists available at ScienceDirect

Journal of Alloys and Compounds

journal homepage: www.elsevier.com/locate/jallcom

Sinterability and electrical properties of ZnO-doped $Ce_{0.8}Y_{0.2}O_{1.9}$ electrolytes prepared by an EDTA–citrate complexing method

Shujun Li, Lin Ge, Haitao Gu, Yifeng Zheng, Han Chen, Lucun Guo*

College of Materials Science and Engineering, Nanjing University of Technology, No. 5 Xinmofan Road, Nanjing, Jiangsu, 210009, PR China

ARTICLE INFO

Article history:
Received 6 May 2010
Received in revised form 8 August 2010
Accepted 15 August 2010

Keywords:
Solid oxide fuel cell
Yttria-doped ceria
ZnO
Sintering aid
EDTA–citrate complexing method

ABSTRACT

The effect of ZnO addition on the sinterability and ionic conductivity of $Ce_{0.8}Y_{0.2}O_{1.9}$ is investigated. $Ce_{0.8}Y_{0.2}O_{1.9}$ is prepared using an EDTA–citrate complexing method in order to further improve its electrical properties. Using a ZnO content over 1 mol %, the sinterability of $Ce_{0.8}Y_{0.2}O_{1.9}$ is significantly improved by reducing the sintering temperature from 1500 to 1350 °C and a relative density of above 95% was achieved. The highest ionic conductivity of 0.0516 S cm^{-1} was obtained at 750 °C for $(YDC)_{0.99}(ZnO)_{0.01}$ sintered at 1350 °C. Pure YDC sintered at 1500 °C, on the other hand, yielded 0.0289 S cm^{-1}.

1. Introduction

Solid oxide fuel cells (SOFCs) have attracted much attention in recent years due to their various potential advantages, including a wide variety of available fuels, inexpensive technology, good durability and highly efficient energy conversion [1–3]. Among the electrolyte materials available, yttria-stabilized zirconia (YSZ) is the most extensively studied and a key component of SOFC systems. However, YSZ-based SOFCs must be operated at high temperatures around 1273 K in order to obtain sufficiently high current densities and good power output. Such high temperatures often lead to problems, such as solid reactions between the components, thermal degradation, and thermal expansion mismatch. Therefore, efforts have been exerted to reduce the operating temperature of such systems, and it has been found that doped ceria electrolytes exhibit superior ionic conductivity at lower temperature ranges (773–973 K) [4–9].

The ionic conductivity of ceria resulting from oxygen vacancies depends on the dopants and their amount [8,10]. It increases significantly when ceria is doped with aliovalent oxides, such as Y_2O_3 and other rare-earth oxides. However, an increasing amount of dopants tends to form a second phase due to solubility limits, resulting in the reduction of conductivity. Generally, the critical dopant concentration of Y_2O_3 to achieve optimum conductivity is approximately 20% [11]. Some doped electrolytes, such as $Ce_{1-x}Gd_xO_{2-y}$ (GDC), $Ce_{1-x}Sm_xO_{2-y}$ (SDC), and $Ce_{1-x}Y_xO_{2-y}$ (YDC), show relatively high oxide ionic conductivity [4,6,12–14]. Considering the high abundance of yttria in these rare-earth elements, yttria-doped ceria (YDC) is a potentially low-cost electrolyte for IT-SOFC.

The EDTA–citrate complexing process is a modified Pechinitype reaction, and a polymerized complex method to synthesize a wide variety of oxide materials [15–17]. Various metal ions in a solution are chelated to form metal complexes. These chelates undergo poly-esterification when heated to form a polymetric glass that has uniformly distributed metal ions. The resultant powders have nano-scaled particle size and high degree compositional homogeneity at the molecular level.

A lower sintering temperature (<1400 °C) is necessary to restrain solid state reactions, diffusions between ceramic materials, and other serious problems. The low activity of sinterability has caused the synthesis of YDC bulk ceramics below 1550 °C to remain a challenge in its application in IT-SOFC [18–20].

Thus far, research on low temperature sintering of ceria-based electrolyte materials have focused mainly on either the synthesis of highly reactive ceramic powder or searches for suitable sintering aids for the solid reaction process. CoO, MnO, CuO, and Al_2O_3 as sintering aids have been found to be effective in improving densification effectively but these have a more or less negative impact on conductivity [21–26]. Very recently, Gao et al. [27] synthesized $(Ce_{0.84}Y_{0.16}O_{1.92})_{1-x}(ZnO)_x$ electrolytes through a solid state reaction using ZnO as the sintering aid and decreased the sintering temperature from 1600 °C (20 h) to 1375 °C (20 h). However the addition of ZnO exhibited a slight detrimental influence on their conductivities.

* Corresponding author. Tel.: +86 25 83587261; fax: +86 25 83306152.
E-mail address: lc-guo@163.com (L. Guo).

0925-8388/$ – see front matter © 2010 Elsevier B.V. All rights reserved.
doi:10.1016/j.jallcom.2010.08.111

In the present work, the effect of ZnO addition on the sinterability and ionic conductivity of $Ce_{0.8}Y_{0.2}O_{1.9}$ prepared using an EDTA–citrate complexing method is investigated. The aim is to improve the sinterability and ionic conductivity of YDC electrolytes.

2. Experimental procedures

2.1. Sample preparation

The $Ce_{0.8}Y_{0.2}O_{1.9}$ (YDC) powders were synthesized using a combined EDTA–citrate complexing method. EDTA ($[CH_2N(CH_2COOH)_2]_2$) was dissolved in $NH_3{\cdot}H_2O$ solution to prepare a $NH_3{\cdot}H_2O$–EDTA buffer solution. Next, calculated amounts of $Ce(NO_3)_4{\cdot}6H_2O$ and $Y(NO_3)_3{\cdot}6H_2O$ were dissolved in the above EDTA–$NH_3{\cdot}H_2O$ solution under heating and stirring. After stirring for a certain length of time, the proper amount of citric acid ($C_6H_7O_7{\cdot}H_2O$) was added. The mole ratio of EDTA, citric acid, and total metal ions was controlled at around 1:1.5:1. $NH_3{\cdot}H_2O$ was added to adjust pH values (around 6) to avoid the occurrence of precipitation after citric acid addition. The solution was continuously stirred and heated at 80 °C. A gold gel was obtained with the evaporation of water. The gelled samples were baked in a drying oven at 120 °C for 48 h. Finally, the dried gel was calcined at 600 °C for 2 h. Different amounts of zinc oxide were added as an appropriate sintering aid. The mixed powders were ball-milled for 12 h using zirconia balls. After drying, the powders were ground with 5 wt.% PVA solution in an agate mortar and die-pressed into cylindrical pellets (14 mm in diameter) under a pressure of about 100 MPa. The green pellets were heated at various temperatures (1250–1500 °C) in air for 2 h and subsequently cooled to room temperature.

2.2. Characterization

Shrinkage and relative density were measured to characterize the sinterability of the specimens. The shrinkage was calculated as follows:

$$\text{Shrinkage}\ (\%) = \frac{L_0 - L_1}{L_0} \times 100\% \quad (1)$$

where L_0 and L_1 are the lengths of the green and sintered specimens, respectively. The densities of the sintered pellets were measured using the Archimedes' method in a water bath.

Phase analysis was performed on the crushed pellet. X-ray diffraction (XRD) experiments were carried out at room temperature on an X-ray diffractometer (XRD, D/max-III, Rigaku) with Cu Kα radiation in the 2θ range of 20–80°. The cross-section micrographs of sintered samples were observed using a scanning electron microscope (SEM, Model JSM-5900, JEP, Tokyo, Japan).

The oxide ionic conductivity of the materials was measured using electrochemical impedance spectroscopy based on sintered pellets. Both sides of the pellets were coated with silver paste as electrodes and fired at 600 °C for 30 min before measurement to ensure good bonding. The as-prepared samples were mounted in an alumina supporter and jigged with Pt wires using ceramic springs. The AC impedance spectra of the pellets were measured over 450–750 °C in air using an impedance analyzer (PARSTAT 2273) over 0.1–100 kHz. Curve fitting and resistance calculations were carried out using ZSimpWin software.

Thermal expansion measurements were conducted with a dilatometer (RPZ-01, Luoyang, China) operated from room temperature to 800 °C in air (heating rate 5 °C/min).

3. Results and discussion

3.1. Sinterability

The linear shrinkage of $(YDC)_{1-x}(ZnO)_x$ sintered at different temperatures is shown in Fig. 1. An enhancement of sinterability was observed with ZnO content up to 1 mol.%; any addition above this level had no significant effect on shrinkage. In the range of 1250–1350 °C, the $(YDC)_{1-x}(ZnO)_x$ systems with $x \geq 0.01$ achieved a certain degree of shrinkage degree at a temperature 150 °C lower than that of pure YDC. Moreover, they all obtained their maximum shrinkage (~20.8%) at 1350 °C, whereas it was only 11% for pure YDC.

Fig. 2 shows the calculated relative densities of samples as a function of sintering temperature. The densities of samples increased gradually with increasing sintering temperature as the result of the minimization of the pores and the growth of the crystal. The difference in sintering behaviors between pure YDC and ZnO-added samples were particularly evident. At the temperature of 1350 °C, the relative densities of the modified systems with ZnO all achieved peak value. A further increase in temperatures showed no obvious disparity in the relative density. The specimen with 1 mol.% ZnO achieved a peak value (98.2%) at 1350 °C, whereas it was only 70% for pure YDC. The samples synthesized with ZnO displayed better sinterability than pure YDC.

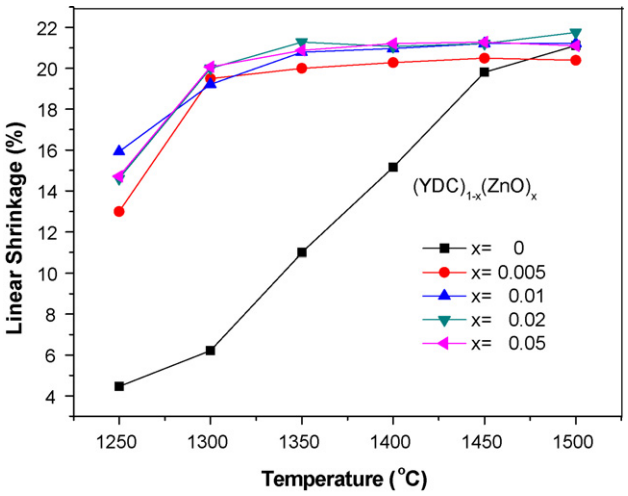

Fig. 1. Shrinkage of $(YDC)_{1-x}(ZnO)_x$ sintered at different temperatures.

3.2. Phase composition and crystal structure

The XRD patterns of YDC calcined at 600 °C for 2 h are shown in Fig. 3. The doped ceria powder crystallite had a single phase with cubic fluorite structure and was similar to pure ceria. No second phase was observed. This may result in better chelation between the constituent cations and EDTA or citrate acid. In the case of a conventional mixed oxide route, the cubic fluorite structure was obtained at 1200 °C [28]. In the present EDTA–citrate complex synthesis process, a single phase of ceria was obtained at 600 °C. Low temperature synthesis was attributed to the uniform distribution and atomic scaled reaction of the metal ions. The reaction of the raw materials under calcined condition can be denoted by the chemical Eq. (2)

$$0.8Ce(NO_3)_3{\cdot}6H_2O + 0.2Y(NO_3)_3{\cdot}6H_2O + 1.2C_6H_8O_7 + C_9H_{16}N_2O_8 \rightarrow Ce_{0.8}Y_{0.2}O_{1.9} + 16.2CO_2\uparrow + N_2\uparrow + 17.6H_2O \quad (2)$$

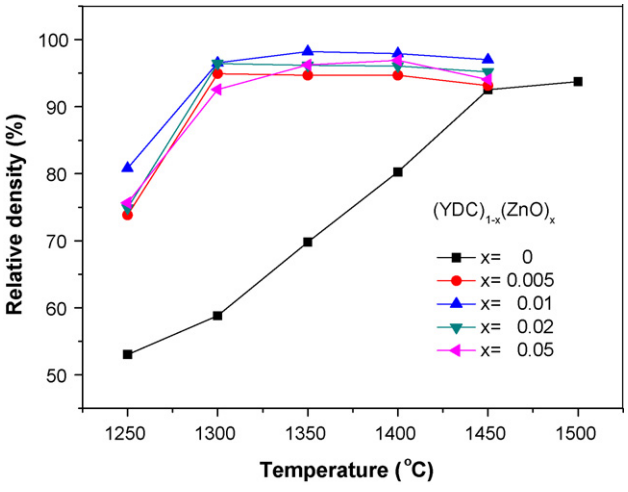

Fig. 2. Relative density as a function of sintering temperature for $(YDC)_{1-x}(ZnO)_x$ sintered at different temperatures.

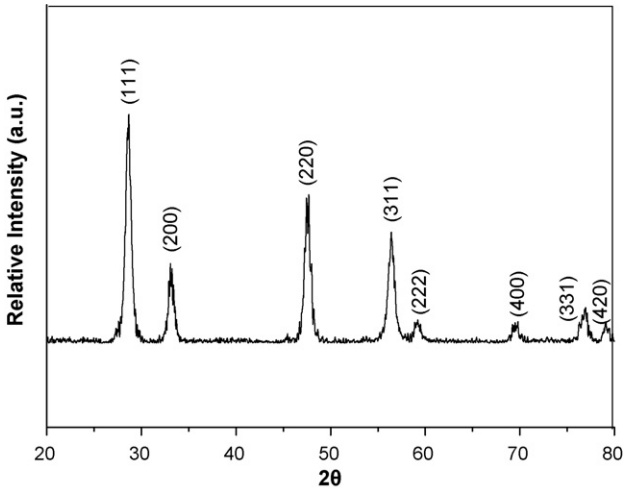

Fig. 3. X-ray diffraction patterns of YDC calcined at 600 °C for 2 h.

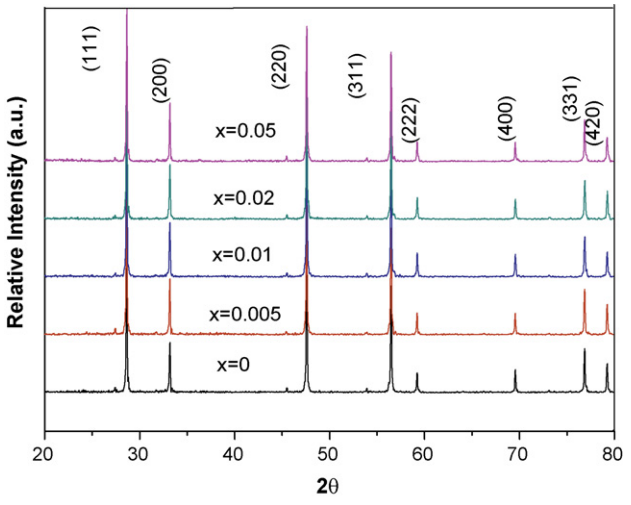

Fig. 4. X-ray diffraction patterns of $(YDC)_{1-x}(ZnO)_x$ ($x = 0.005$, 0.01, 0.02, and 0.05) sintered at 1350 °C for 2 h and pure YDC ($x = 0$) at 1500 °C for 2 h.

Fig. 4 displays the XRD patterns of the $(YDC)_{1-x}(ZnO)_x$ samples sintered at 1350 °C ($x = 0$, 1500 °C). For the same pressing condition and sintering regime, all the compositions studied were single phase of ceria with an Fm3m cubic fluorite structure. This suggests that fine powders synthesized using EDTA–citrate complexing method can be sintered successfully into electrolytes with a single phase. Negligible change was found from the position of the diffraction peaks for the samples doped by ZnO compared to those of the undoped sample because of the small solid solubility of ZnO in YDC [27]. There were some small peaks on the left of the (1 1 1), (2 0 0), (2 2 0), and (3 1 1) peaks. Further analysis showed that these small peaks were consistent with the diffraction peaks of SiO_2 and Al_2O_3. This is mainly because we used a ceramic mortar to crush the pellets and grind them into powders during the preparation of the samples for phase analysis. The hardness of the samples caused a mix of tiny mortar powder with SiO_2 and Al_2O_3 as main components.

3.3. Microstructure

Fig. 5 shows the SEM photographs of $(YDC)_{1-x}(ZnO)_x$ sintered at different temperatures. The sample without ZnO ($x = 0$) was found to be very porous despite being sintered at 1500 °C. In contrast, the sample with 1 mol.% ZnO was very dense with small closed pores, which was in agreement with the results of shrinkage (Fig. 1) and relative density (Fig. 2). The rapid densification of ZnO-added specimens may be attributed to a liquid-phase sintering mechanism. The presence of a liquid formed by ZnO at the sintering temperature can enhance densification during sintering of these samples, as indicated in previous reports [27].

3.4. Ionic conductivity

Ionic conductivity of $(YDC)_{1-x}(ZnO)_x$ was measured by means of electrochemical AC impedance spectroscopy. The AC impedance included the contribution of the grain interior, grain boundaries, and electrode–electrolyte. Typical Nyquist representations and equivalent circuit model of $(YDC)_{0.99}(ZnO)_{0.01}$ (1350 °C, 2 h) measured at 200 °C are shown in Fig. 6. The small arc in the left (shown in the inset figure) can be attributed to grain interior polarization (high frequency). The broad arc in the middle is ascribed to the

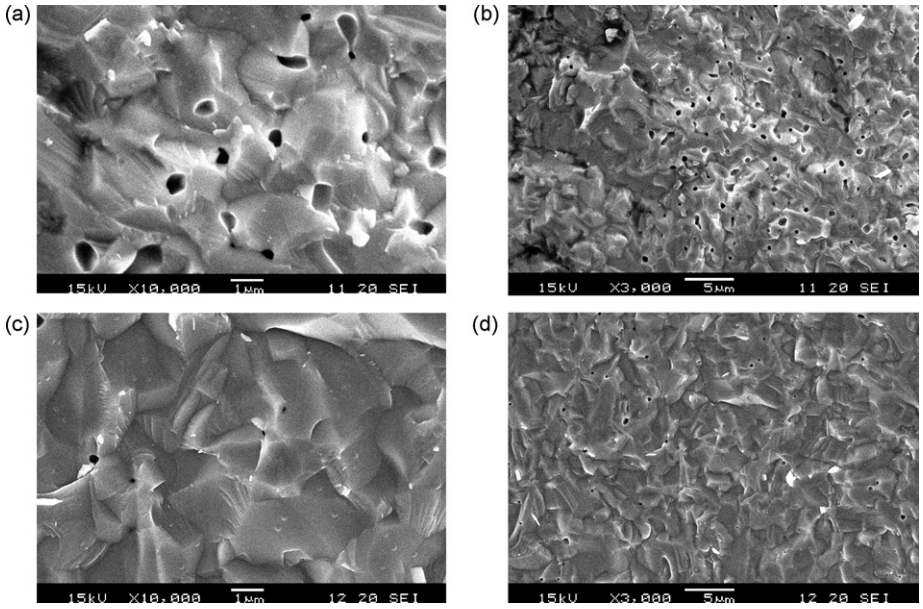

Fig. 5. SEM photographs of $(YDC)_{1-x}(ZnO)_x$: (a), (b) $x = 0$, sintered at 1500 °C for 2 h; (c), (d) $x = 0.01$, sintered at 1350 °C for 2 h.

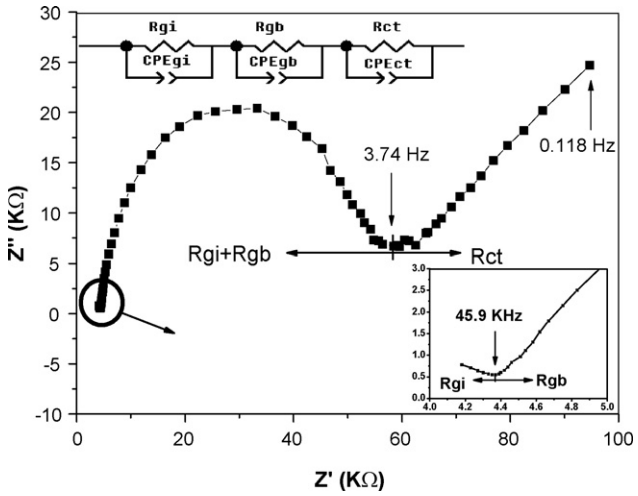

Fig. 6. Impedance spectra and equivalent circuit of $(YDC)_{0.99}(ZnO)_{0.01}$ sintered at 1350 °C for 2 h. The inset shows an enlargement of the high frequency district. $T = 200$ °C.

grain boundary polarization (intermediate frequency), and the last arc in the right is due to the electrode polarization (low frequency). R_{gi}, R_{gb}, and R_{ct} represent the grain interior resistance, grain boundary resistance, and electrode resistance, respectively. In the present case, in order to model an experimental data, the capacitor was replaced by a constant phase element (CPE) that accounted for the microstructure inhomogeneity within the sample and was equivalent to a distribution of capacitors in parallel. CPE_{gi}, CPE_{gb}, and CPE_{ct} refer to the constant phase element of grain interior, constant phase element of grain boundary, and constant phase element of electrode, respectively.

The total resistance of electrolyte can be expressed as:

$$R_t = R_{gi} + R_{gb} \tag{3}$$

The total conductivity at different temperatures could be calculated using the equation:

$$\sigma_t = \frac{1}{R_t} \cdot \frac{L}{S} \tag{4}$$

where L and S represent sample thickness and electrode area of the sample surface, respectively.

Fig. 7 shows Arrhenius plots of the total ionic conductivity for the ZnO-doped samples at temperature from 450 to 750 °C with different x (zinc oxide concentration) in the form of $\ln(\sigma T)$ versus $1000/T$. As a contrast, the data of pure YDC sample ($x = 0$) sintered at 1500 °C were also included. The measured conductivity data were analyzed using the traditional Arrhenius equation:

$$\sigma = \frac{A}{T} \exp\left(-\frac{E}{kT}\right) \tag{5}$$

where E is the activation energy of electrical conduction, k is the Boltzmann's constant, T is the absolute temperature, and A is the pre-exponential factor, which is a constant at certain temperature range. For $(Ce_{0.8}Y_{0.2}O_{1.9})_{1-x}(ZnO)_x$ ($x = 0.005$, $x = 0.01$, $x = 0.02$, $x = 0.05$), the ionic conductivity increased from $x = 0.005$ to $x = 0.01$ then decreased. The highest ionic conductivity of 0.0516 S cm^{-1} was obtained at 750 °C for $(YDC)_{0.99}(ZnO)_{0.01}$ sintered at 1350 °C. Pure YDC sintered at 1500 °C yielded 0.0289 S cm^{-1}. The ionic conductivity of $(YDC)_{0.99}(ZnO)_{0.01}$ was observed to be much higher than that of pure YDC ($x = 0$). The above analysis ascertained that YDC with an optimum ratio of ZnO could improve the electrical property of ceria electrolytes further. Optimum composition was observed with $x = 0.01$. The highest ionic conductivity was 0.0516 S cm^{-1} at 750 °C, which was higher than the previous results wherein the highest ionic conductivity was below 0.04 S cm^{-1} at 750 °C [27]. The study demonstrated that better electrical properties could be obtained with samples synthesized by the EDTA–citrate complexing method in this study. Although $(YDC)_{0.99}(ZnO)_{0.01}$ was still not well sintered, the cross-section micrograph in Fig. 5 revealed some closed pores, showing a not-fully densified microstructure, that is consistent with the relative density values being less than 100%. Thus, it can be concluded that sinterability of the specimens can be promoted further by prolonging the holding time, whereas ionic conductivity may be improved by increasing the density. We will discuss this part in our next work.

Fig. 8 gives the activation energy values of $(YDC)_{1-x}(ZnO)_x$ electrolytes at the temperature range of 450–750 °C, clearly indicating that $(YDC)_{0.995}(ZnO)_{0.005}$ exhibited the highest activation energy and $(YDC)_{0.995}(ZnO)_{0.01}$ the lowest and is in good agreement with Fig. 7.

The optimized amount of ZnO facilitated the improvement of ionic conductivity for $(YDC)_{0.99}(ZnO)_{0.01}$. All the samples were composed of single phases of ceria with an Fm3m cubic fluorite structure according to the analysis of XRD patterns shown in Fig. 4;

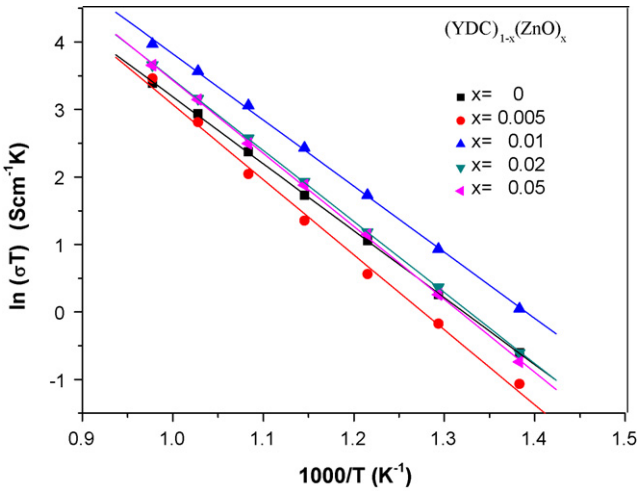

Fig. 7. Arrhenius plots for the ionic conductivities of $(YDC)_{1-x}(ZnO)_x$ ($x = 0.005$, $x = 0.01$, $x = 0.02$, $x = 0.05$) sintered at 1350 °C for 2 h and pure YDC ($x = 0$) at 1500 °C for 2 h.

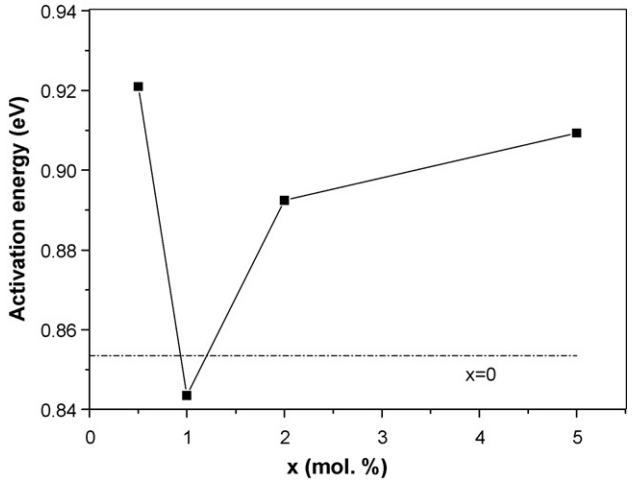

Fig. 8. Activation energy of $(YDC)_{1-x}(ZnO)_x$ ($x = 0.005$, $x = 0.01$, $x = 0.02$, $x = 0.05$) sintered at 1350 °C for 2 h and pure YDC ($x = 0$) at 1500 °C for 2 h at the temperature range of 450–750 °C.

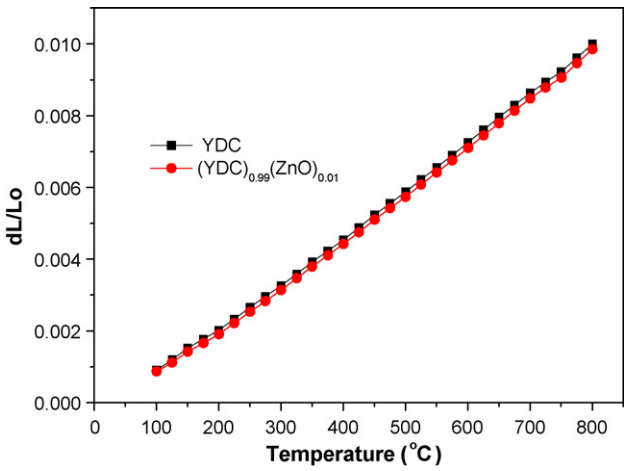

Fig. 9. Linear thermal expansion curves for $(YDC)_{0.99}(ZnO)_{0.01}$ sintered at 1350 °C for 2 h and pure YDC at 1500 °C for 2 h.

hence, the different ionic conductivity could not be ascribed to the phase discrepancy, but rather to the difference in sintering and microstructure. The higher ionic conductivity and lower activation energy for the $(YDC)_{0.99}(ZnO)_{0.01}$ sample could probably be attributed to the higher density (shown in Fig. 2) and the more compact arrangement of crystal grains (shown in Fig. 5) that favored the transportation of the carriers.

In this study, for the samples of $(YDC)_{1-x}(ZnO)_x$ electrolytes, doping with ZnO may cause two opposite effects. On the one hand, as a sintering aid, ZnO can reduce porosity and improve sinterability to effectively obtain a dense electrolyte material, leading to a decrease in activation energy of conduction and an increase in ionic conductivity. On the other hand, ZnO also shows a detrimental influence on conductivity [16–21], which leads to an increase in the activation energy of conduction and a decrease in ionic conductivity. When the ZnO content (x) was at 0.5 mol.%, the latter effect may be stronger than the former, resulting in lower ionic conductivity and higher activation energy for conduction. However, when the dopant content (x) was at 1 mol.%, the former effect may be stronger than the latter, leading to higher ionic conductivity and lower activation energy for conduction.

3.5. TEC measurements

Fig. 9 shows the thermal expansion curves of pure YDC and $(YDC)_{0.99}(ZnO)_{0.01}$ samples, with both samples showing linear temperature dependence. The thermal expansion coefficients (TECs) between 100 and 800 °C were calculated from the curves. The TEC of pure YDC was $12.9 \times 10^{-6}\ K^{-1}$, whereas it was $12.7 \times 10^{-6}\ K^{-1}$ for $(YDC)_{0.99}(ZnO)_{0.01}$. The values indicate that the addition of 1 mol.% ZnO did not change the TECs of YDC significantly and that they may therefore be compatible with each other.

4. Conclusions

The EDTA–citrate complexing method can synthesize samples with better electrical properties. As an effective sintering aid, ZnO effectively lowered the sintering temperature of YDC electrolyte from 1500 to 1350 °C. For $(YDC)_{1-x}(ZnO)_x$ ($x = 0.01$, $x = 0.02$, $x = 0.05$), ionic conductivity was improved in comparison to pure YDC, and the highest ionic conductivity was 0.0516 S cm^{-1} at 750 °C with $x = 0.01$. It was confirmed that an appropriate amount of ZnO could improve not only the sinterability but also the ionic conductivity of $Ce_{0.8}Y_{0.2}O_{1.9}$ electrolytes.

Acknowledgement

We would like to thank the Jiangsu Provincial Key Laboratory of Inorganic and Composite Materials.

References

[1] V. Verda, M. Cali Quaglia, Int. J. Hydrogen Energy 33 (2008) 2087–2096.
[2] B. Lin, S.L. Wang, X.Q. Liu, G.Y. Meng, J. Alloys Compd. 490 (2010) 214–222.
[3] S.K. Lee, K.H. Kang, H.S. Hong, Y.S. Yun, J.H. Ahn, J. Alloys Compd. 488 (2009) L1–L5.
[4] L.D. Jadhav, M.G. Chourashiya, K.M. Subhedar, A.K. Tyagi, J.Y. Patil, J. Alloys Compd. 470 (2009) 383–386.
[5] B.C.H. Steele, Solid State Ionics 129 (2000) 95–110.
[6] S. Dikmen, J. Alloys Compd. 491 (2010) 106–112.
[7] D. Hari Prasad, H.R. Kim, J.S. Park, J.W. Son, et al., J. Alloys Compd. 495 (2010) 238–241.
[8] M. Mogensen, N.M. Sammes, G.A. Tompett, Solid State Ionics 129 (2000) 63–94.
[9] J.S. Lee, K.H. Choi, M.W. Park, Y.G. Choi, J.H. Mun, J. Alloys Compd. 474 (2009) 219–222.
[10] H. Inaba, H. Tagawa, Solid State Ionics 83 (1996) 1–16.
[11] T.S. Zhang, J. Ma, L.B. Kong, S.H. Chan, J.A. Kilner, Solid State Ionics 170 (2004) 209–217.
[12] E.C.C. Souzaa, E.N.S. Muccillo, J. Alloys Compd. 473 (2009) 560–566.
[13] K. Eguchi, T. Setoguchi, T. Inoue, H. Arai, Solid State Ionics 52 (1992) 165–172.
[14] G.B. Balazs, R.S. Glass, Solid State Ionics 76 (1995) 155–162.
[15] Z.P. Shao, S.M. Haile, Nature 431 (9) (2004) 170–173.
[16] Z.P. Shao, W.S. Wang, Y. Cong, H. Dong, J.H. Tong, G.X. Xiong, J. Membr. Sci. 172 (2000) 177–188.
[17] X.F. Ding, Y.J. Liu, L. Gao, L.C. Guo, J. Alloys Compd. 458 (2008) 346–350.
[18] R.T. Dirstine, R.N. Blumenthal, T.F. Kuech, J. Electrochem. Soc. 126 (1979) 264–269.
[19] C. Pascual, J.R. Jurado, G.F. Arroyo, L. Del Olmo, C. Moure, P. Duran, Sci. Ceram. 12 (1984) 729–734.
[20] T.S. Zhang, J. Ma, H.T. Huang, P. Hing, Z.T. Xia, S.H. Chan, J.A. Kilner, Solid State Sci. 5 (2003) 1505–1511.
[21] C. Kleinlogel, L.J. Gauckler, Solid State Ionics 135 (2000) 567–573.
[22] T.S. Zhang, J. Ma, L.B. Kong, P. Hing, Y.J. Leng, S.H. Chan, J.A. Kilner, J. Power Sources 124 (2003) 26–33.
[23] T.S. Zhang, P. Hing, H.T. Huang, J. Kilner, Mater. Lett. 57 (2002) 507–512.
[24] T.S. Zhang, L.B. Kong, Z.Q. Zeng, H.T. Huang, P. Hing, Z.T. Xia, J. Kilner, J. Solid State Electrochem. 7 (2003) 348–354.
[25] T.S. Zhang, Z.Q. Zeng, H.T. Huang, P. Hing, J.A. Kilner, Mater. Lett. 57 (2002) 124–129.
[26] M. Mori, E. Suda, B. Pacaud, K. Murai, T. Moriga, J. Power Sources 157 (2006) 688–694.
[27] L. Gao, M. Zhou, Y.F. Zheng, H.T. Gu, H. Chen, L.C. Guo, J. Power Sources 195 (2010) 3130–3134.
[28] Y.F. Zheng, L.Q. Wu, H.T. Gu, L. Gao, H. Chen, L.C. Guo, J. Alloys Compd. 486 (2009) 586–589.